出芽酵母非必須遺伝子破壊株の形態情報に基づく薬剤作用標的の探索

岡　さとみ

東京大学大学院新領域創成科学研究科
先端生命科学専攻

２００６年

修士論文

Discovering biological targets for drug action using comprehensive morphological data of genome-wide yeast deletion mutants

Satomi Oka

Department of Integrated Biosciences
Graduate School of Frontier Sciences
The University of Tokyo

2006

Master Thesis

Table of Contents

List of Figures

List of tables

Acknowledgements

I wish to express my deepest gratitude to an outstanding and experienced Geneticist, Prof. Yoshikazu Ohya for his supervision and advice throughout this study.

I also wish to express my gratitude to Associate Prof. Kintake Sonoike for his insightful suggestions and patient encouragement throughout this study.

I thank Dr. Nogami Satoru, Dr. Masashi Yukawa and Dr. Fumi Sano for their helpful advice, discussion and encouragement.

I would also like to express my sincere gratitude to Shinsuke Ohnuki for great help.

I would like to thank Emi Shimoi, Yuka Kitamura, and Tamao Goto for their technical support.

I would like to thank Prof. David G. Drubin providing the *act1 ts* mutants.

I also thank all members of laboratory of Department of Integrated Biosciences Graduate School of Frontier Sciences, for their encouragement.

I am grateful to Miyuki Imanari, Hiroyuki Usuki and Machika Watanabe for their mental supporting.

Last but not least, I also thank my family for mental and financial support.

Abbreviations

DAPI: 4', 6-Diamidino-2-phenylindole

EUROFAN: the European *Saccharomyces cerevisiae* Archive for Functional Analysis

FITC-ConA: fluorescein isothiocyanate/concanavalin A

GO: gene ontology

HU: hydroxyurea

LAT-A: latrunculin A

PBS: phosphate buffered saline

PCR: polymerase chain reaction

Rh-ph: Rhodamine-phalloidin

SCMD: *Saccharomyces Cerevisiae* Morphological Database

SGD: *Saccharomyces* Genome Database

WT: wild type

YPD: 1% yeast extract, 2% bactopeptone, 2% glucose

Summary

"Chemical Genetics" is an emerging approach to study gene-product functions using chemical compounds. In order to get more information about gene-product functions impaired by the drugs, it is necessary to elucidate the targets of the drugs. Taking that chemical compounds are frequently used for a therapeutic purpose, discovering the targets of the drugs is very important for its utilization both in therapeutic and experimental tools. However, there are few definitive general methods for identifying the drug targets based on genome-wide analyses. In our laboratory, to describe the yeast phenotype objectively and quantitatively, an image-processing program, named CalMorph was developed (Ohtani *et al.*, 2004), accumulating comprehensive morphological data of yeast mutants. Here, by using this morphological database, I propose a novel strategy to identify the deletions of the target genes by searching the similar morphological phenotype after the drug treatment. To demonstrate the efficacy of this protocol, I tested its validity with well-characterized drugs such as hydroxyurea (HU: a non-alkylating myelosuppressive agent that inhibits DNA synthesis) and latrunculin A (LAT-A: an inhibitor of the assembly step in a rapid cycle of binding to monomeric G-actin). In both cases, morphological phenotypes of the drug-treated cells resemble those of the mutant cells defective in their target proteins. The results imply that it is possible to discover biological targets for drug action using comprehensive

morphological database of the yeast deletion mutants. This novel method is theoretically applicable to identify any gene products that functionally interact with small molecules, and therefore will generally provide powerful techniques for inferring mechanism of the drug action.

Introduction

Small-molecules that perturb specific protein functions are valuable tools for dissecting complex processes in cells. Many small-molecules have been repeatedly used to elucidate the biological phenomena. On the other hand, administration of medicine is very powerful therapy to cure patients of various diseases. From 19th century, the active ingredients of medicinal plants have been isolated, purified and also demonstrated its value for medicine. However, many drugs currently in use were discovered without knowledge of their underlying molecular mechanisms. Understanding their biological targets and modes of action will be essential to use them more effective and more efficiently. Thus, it is one of the most important steps for both biologist and clinicians to identify the drug-target. However, there is no tool that can efficiently identify the protein targets of small molecules with interesting biological properties. To overcome the difficulty to elucidate the target of drugs, many scientists have been used chemical genetics approach over the past decade (Zewail *et al.*, 2003, Dolma *et al.*, 2003). The advent of molecular biology and, in particular, of genomic sciences is having a deep impact on drug discovery. Chemical Genetics (Schreiber et al., 1999) is an emerging research field that utilizes biologically active small molecules to determine the target of each chemical and to study biological functions of the target gene products. This approach shares much in common with the science of genetics. Forward genetics entails

introducing random mutations into cells, screening mutant cells for a phenotype of interest and identifying mutated genes in affected cells. Reverse genetics entails introducing a mutation into a specific gene of interest and studying the phenotypic consequences of the mutation in a cellular context. On the other hands, forward chemical-genetics entails screening small molecules in cells, selecting a drug that induces a phenotype of interest, and identifying the protein target of this drug. Reverse chemical-genetics entails over-expressing a protein of interest, screening for a compound for the protein, and using the chemicals to determine the phenotypic consequences of altering the function of this protein in a cellular context. Although this approach is especially important for studying higher eukaryotes and for pharmacological intervention of human diseases, it remains a formidable task to find small-molecules that alter the function of macromolecules with both sensitivity and specificity. However, if the potential drug targets were components required for cell division or DNA repair, where there is significant conservation of function between humans and yeast, then yeast would be the organism of choice. Furthermore, yeast which is unicellular organism is highly amenable to genetic manipulations.

Taking relatively simple ellipsoidal shape and possessing the conserved basic cellular processes, *Saccharomyces cerevisiae* has been traditionally used for the study. In 1996, the decoding of *S. cerevisiae* genome sequence was completed (Goffeau *et al*), and it was demonstrated that the budding yeast genome is composed of about 1200

essential genes and about 5000 non-essential genes. The availability of complete genome sequences has yielded the ability to perform high-throughput, genome-wide screens of gene function. The *Saccharomyces* Genome Deletion Project Consortium has constructed the set of those non-essential gene disruptants in 1999 (Winzeler et al.). Using this collection, various phenotypic analyses, such as cell shape (Giaever *et al.*, 2002.) and centromere cohesion (Marston *et al.*, 2004.), have been performed individually under the microscopy. Like these studies, large differences in a specific morphology, such as cell size, cell shape and bud site pattern between wild-types and mutants are able to be distinguished by the visual screening. However, the extracted information from these screenings has the limitation to get more information in detail. Furthermore, to elucidate the gene function and the cellular mechanism, cell morphology is one of the most classic and powerful tools. It was necessary to have developed quantitative and objective techniques that obtain more information for the study of cellular mechanisms. Then, to describe the phenotype objectively, CalMorph was constructed as an image-processing program to extract various morphological data from digital images representing actin cytoskeleton, cell wall and nucleus microscopic images (Ohtani *et al.*, 2004.). By analyzing all 4718 non-essential gene deleted mutants with this program, we can extract 501 quantitative morphological data (Ohya *et al.*, 2005).

Recent technological advances in yeast genomics, including quantitative

phenotype profiling and analysis of drug induced gene expression change (Hughes et al., 2000), show promise for the rapid development in the study of proteins and pathways affected by drugs at a genome-wide level. In 2004, the efficacy of genome-wide protocols using chemicals with the complete collection of heterozygous yeast deletion strains allowed the identification of those gene products that functionally interact with small molecules. However the indication for identification was only cell growth (Giaever *et al.*2004, Lum *et al.*2004, Beazs *et al.*2004). If there are more indicators of the changes that are led by compounds, the study of the yeast deletion strains collection is more effective to understand the target of drug.

To overcome this problem, I recruit the high-dimensional phenotyping technique. Because a loss-of-function mutation in a gene encoding the target of an inhibitory compound models the primary effect of the compound (Hughes et al., 2000), it is plausible to detect the mutant showing similar phenotype to the drug-treated cells. In this study, I proposed novel strategy to detect the target gene deletions by searching the similar phenotype of drug treatment cells from genome-wide yeast mutants in morphological database (SCMD http://scmd.gi.k.u-tokyo.ac.jp/datamine/) (Saito *et al.*2004). To establish this proof of concept, I applied a novel strategy with well-characterized compounds to their target pathways and proteins.

Result and discussion

I. Confirmation of correct gene KO in the cell morphology mutants

In our laboratory, we use *MATa* deletion strains collection purchased from EUROFAN. For comprehensive analysis of quantitative data about the cell morphology mutants, it is important to show that each deletion strain has correct gene knockout. To test this, I individually checked the deleted genes by PCR amplification using AI/KanB primer and upstream primer of each gene (shown in **Table 2**).

II. Novel strategy for discovering the target of the drugs

To know the intracellular targets affected by the natural and synthetic compounds, Giaever (2002) demonstrated the efficacy of a genome-wide approach. Her protocol allows the identification of the gene products that functionally interact with the drugs, based on the information about the inhibition of cellular proliferation in the specific yeast mutants. However, providing more indicators for assessment of the drug function should be powerful. To cover this, I propose alternative protocol that uses the results of high-dimensional quantitative morphological analysis

1.Premises for the novel strategy

First of all, we made the following assumptions (**Figure 1**):

Premise 1. The phenotype due to the drug-treatment is caused by impairment of

the specific drug-target.

1-a) The phenotypic change induced by the drug resembles the one caused by impairment of the specific drug-target.

1-b) The phenotypic change caused by the gene deletion is more remarkable than the one by the drug-treatment.

1-c) Deletion of the drug target gene results in alteration in most of the phenotypic parameters that are affected by the drugs.

Premise 1-a) and 1-c) can be inferred from Premise1. Premise 1-b) can be inferred from Premise1 and the following Premise 2.

Premise 2. Drug concentration correlates with the values in the affected phenotypic parameters.

2.Introduction of Novel strategy

The above assumptions are used to develop the experimental strategy to detect the target of the drugs as outlined in **Figure 2**. For CalMorph analysis, wild-type cells are cultured in the drug presence YPD medium(**Figure 2; 1,2**) and the morphology of these cells are derived along with manual of CalMorph (**Figure 2; 3-6**). The parameters which have significant values between the drug-treated cells and control cells are extracted with "U"-test (**Figure 2; 7**). Then, the parameters which change values in drug-concentration dependent manner are selected (**Figure 2; 8**). And these mutants are regarded as

candidate coding the drug-target (**Figure 2; 9**). To check the availability of this prediction, I verified the strategy by the well-characterized drugs (HU and LAT-A)(**Figure 3**) as a pilot study. HU has been reported as a non-alkylating myelosuppressive agent that inhibits DNA synthesis by inhibition of ribonucleoside-diphosphate reductase small subunit of Rnr2p and Rnr4p (Barlow *et al.*, 1983) (**Figure 4**). LAT-A has been known as an inhibitor of the assembly step in a rapid cycle of binding to monomeric G-actin in a 1:1 complex (Ayscough *et al.*, 1999, Morton et al., 2000) (**Figure 5**) Actin is coded by *ACT1*.

HU

Examination of appropriate concentration of HU

The minimum inhibitory concentration (MIC) or 50% inhibitory concentration (IC50) usually gives an indication of the potency of the drugs. However, these concentrations may not be suitable for analysis of drug-induced phenotypic alteration. In order to examine the optimal drug-concentration for this analysis, I checked growth rate in the presence of various concentration of HU against the wild-type strain (BY4741). To exclude the side effect of the drug as much as possible, I focused on the minimum inhibitory concentrations that lead to phenotypic changes. The growth curve of the wild-type cells in the presence of HU is shown in **Figure 6**. HU-Treatment with the concentration below 5 mM did not inhibit the cell growth but the one with above 30

mM HU inhibited cell growth. According to these results, I decided to analyze the phenotypes at the HU concentrations ranging from 5 to 30 mM.

Quantitative morphological data of the drug-treated cells

Cells were grown in YPD medium with the drug (5, 10, 20 and 30 mM HU) or DMSO (as a control) for 8 hours, and were fixed with formaldehyde. To obtain fluorescent images of the cell wall, actin cytoskeleton and nuclear DNA, the cells were triply stained with FITC-concanavalin A (FITC-ConA), rhodamine-phalloidin (Rh-ph) and DAPI, respectively, and observed by fluorescent microscopy (**Figure 7**). After each image was captured, each cell was automatically recognized by CalMorph (**Figure 8**), and the values of 79 basic parameters were obtained (**Figure 15**). Based on these basic parameters, the values of 501 morphological parameters were calculated and displayed within the columns of Excel sheet (data not shown).

Significant phenotypic alteration in the presence of HU

To describe the significant phenotypic alteration by the drugs in a statistically sense, I used "U"-test. In the "U"-test, each treated entity is compared to each control entity. When "U"-test is used for detection of the significant differences between the drug treatment cells and normal cells, five experimental trials are at least required (Ohnuki, unpublished data). Five independent experiments were performed for each drug

concentration and these treated entities and the control entity data were compared. To exclude the side effect, I adopted the data of the cells treated with lower concentration compound to compare with control cells. Results show that the values of the 25 parameters (**Figure 9**) were significantly altered ($P < 0.001$) in the presence of 5 mM HU.

Detection of the parameters whose values are correlated with the drug concentration

The Premise 2 secures that the values in the drug-affected parameters correlate with the drug concentration. To know such drug-affected parameters, the parameters which had strong positive and negative correlation ($r > 0.8$, $r < -0.8$) between the drug-concentration and the parameter value were selected. Accordingly, I found that the 24 out of the 25 altered parameters exhibit strong correlations (**Figure 9**). I considered these parameters reflected the effect of HU.

The mutants list of showing abnormal phenotypes

The acquisition of morphological information on all non-essential gene disruptant were finished in 2005, and these data are opened on the data base, called SCMD. Based on premise 1-b), the deletion mutants showing more abnormal phenotypes than the drug-treated cells were searched. The data of the cells treated with higher HU concentration

(30 mM HU) was adopted to select the mutants that resemble the target gene destruction. Deleted mutants with a higher value than the drug-treated cells in each significantly-altered parameter were detected. In the consequence, there were many significant abnormal mutants. And, those variants were ranked in high abnormal order (**Table 4**). Surprisingly, *rnr4*, which is a mutation of the target of HU, showed more abnormal phenotype than the drug-treated cells in all of the 24 parameters (**Figure 10**). This result indicates the morphological phenotype of *rnr4* resembles that of HU-treated cells. Thus, I considered this novel method could have ability to detect the target of drug. On the other hand, Rnr2p which is the main component of ribinucleoside-diphosphate reductase could not be detected. Because Rnr2p is essential for proliferation, this strategy could not discover this target.

LAT-A

To examine the optimal drug-concentration, I checked growth rate of the wild-type strain in the presence of various concentration of LAT-A. The growth curve of wild-type cells in the presence of LAT-A (0.1, 0.5, 1 and 1.5 μM LAT-A) is shown in **Figure 11**. At the concentration of below 0.1 μM, LAT-A-reatment failed to affect the cell growth at more than 1.5 μM concentration it inhibited cell growth. According to these results, I decided to analyze the phenotypes at the LAT-A concentrations ranging from 0.1 to 1.5 μM. The images of LAT-A-treated cells were obtained (**Figure 8**) and analyzed by

CalMorph. Examination with "U"-test revealed that the values of the 29 parameters (**Figure 12**) are significantly altered ($P < 0.001$) in the presence of 0.1 μM LAT-A. Then, I found that the 8 out of the 29 altered parameters exhibit strong correlations with the drug-concentrations (**Figure 12**). Using morphological database, I searched deletion mutants that showed more severe phenotypes than the drug-treated cells (**Table 5**), but there was no mutant showing abnormality in all significantly altered 8 parameters. It is noted that the target of LAT-A, *ACT1* was shown genetically to be an essential gene (Shortle *et al.*, 1982), and that the morphological database of yeast haploid strains has the information of only non-essential gene deletions. To demonstrate the specific target of LAT-A, I took advantage of a congenic collection of actin mutants which was generated by a charge-to-alanine mutagenesis scan of *ACT1* (Shortle *et al.*, 1984, Wertman *et al.*, 1992). Especially, I focused on the *act1* alleles (*act1-112, act1-113, act1-117 and act1-157*) showing resistance to LAT-A. Then, to investigate the possibility that morphological change was due to disruption of normal LAT-A binding site on the actin molecules, I compared the morphlogical phenotypes between *ACT1* alleles and the drug-treated cells. To quantitatively and systematically describe the morphology of the *act1 ts* mutants, I employed fluorescent-image processing program (**Figure 13**). As *act1 ts* mutant and strains of EUROFUN have different background, the value of *ACT1* and *his3Δ* were normalized. Data sets of *act1 ts* mutants and all nonessential mutants value in former parameters were plotted in teardrop view (**Figure**

14). At every all parameters except DCV108_C, some of *act1* mutants have more abnormal value than *ACT1*. *act1-113* showed slightly abnormal phenotypes and, conversely, *act1-112* had strong abnormal phenotypes. This implied that *act1* alleles do not tend to change phenotype in the same way. Comparison of wild-type and *act1* mutants in significantly altered 8 parameters were shown in **Table 6**. When I counted the number of the altered parameter of *act1* mutants, I found that each *act1* mutant showed severe alteration in these morphological parameters (*act1-112*, 8; *act1-113*, 5; *act1-117*, 3; *act1-157*, 5) than the non-essential gene mutants: the average of the non-essential gene disruptants were 1.8. This result suggested the phenotypic change of *act1* mutants resemble that of LAT-A effect. Especially, *act1-112* exhibited 8 remarkable phenotypes in 8 parameters. These data led the fact that the phenotypes of *act1-112* are highly similar to that of drug-treated wild-type cells. As shown in **Table 5**, the some non-essential gene deletion mutants were ranked higher than *act1* mutant. However, these non-essential gene deletions have pleiotropic phenotypes, these pleiotropic phenotypes indicated that these selected mutants showed nonspecific phenomena of LAT-A effect. In conclusion, *act1-112* is very similar to the cells treated with LAT-A. Although the target of LAT-A is essential gene product, I could pursue the target using point mutated strains in more detail. In case the drug-target is essential gene product, these results indicated this approach is informative

In this work, I could detect the biological target of HU; ribonucleoside-

diphosphate reductase inhibitor and LAT-A; actin polymerization inhibitor to utilize novel strategy. Given that this pilot study using well-characterized drugs raised the possibility of discovering the target of compounds, I believe that this strategy is suitable for the screening of drug target. Additionally, when the drug target is the product of essential gene, this novel method is useful to detect the target using conditional mutants.

In summary, I could characterize the morphological parameters which were affected by well-characterized drug. And also, the current study provides that it is possible to discover biological target for drug action using comprehensive morphological data of genome-wide yeast deletion mutants. I expect that investigation on the morphological differences by this novel strategy will help to an interaction between a novel drug and biological substances in vivo. In addition, this study indicates that there is intimate relation between yeast cell morphology and its gene function and that this approach might be a tool for estimation of gene function. I expect that investigation on the morphological differences by our objective methods will help to establish a new insight of the regulation network for cell morphology in living cells.

Materials and Methods

Yeast strains and growth conditions

Strains used in this study are shown in **Table 1**. In this study, *Δhis3* strain was used as a wild-type. Cells were grown in YPD medium or drug containing medium at 25 °C as described in CalMorph user manual. Cells samples were taken in the log-phase of growth (4_10^6 ~ 1_10^7 cells/ml). *ACT1* alleles were given by Botstein labs. Only DDY1537 was diploid cell. To analyze the morphology by CalMorph, *ACT1/act1-157* was sporulated and */act1-157::HIS3* meiotic progeny was identified by tetrad analysis.

Genetic manipulations and recombinant techniques

Crossing, sporulation, and tetrad analysis were carried out described by Rose *et al.* (1989). For amplification of DNA by PCR, TaKaRa Ex TaqTM (TaKaRa Biochemicals, Shiga) was used.

Media

Media for yeast: YPD medium contained 1% Bacto-yeast extract (Difco Laboratories, Detroit, MI), 2% polypeptone (Daigoeiyou Chemicals, Osaka) and 2% glucose (Wako Chemicals, Tokyo). Plates were dried for a few days at room temperature before I use.

Chemicals

HU is a non-alkylating myelosuppressive agent that inhibits DNA synthesis by inhibition of ribonucleoside-diphosphate reductase small subunit of RNR2p, and RNR4p (Barlow *et al.*, 1983). LAT-A prevents the assembly step in a rapid cycle of assembly and disassembly by binding to monomeric G-actin in a 1:1 complex at submicromolar concentrations (Ayscough *et al.*, 1997.). Stock solution of HU [2 M] was made in DW and stock solution of Latrunculin A [10 mM] was made in DMSO.

Estimations of Drug concentration

Concentrations of compounds screened were based on prescreens against a wild-type strain. To exclude the side effect of the drug as much as possible, I focused on the low concentrations that begin to induce phenotype change. Until the doubling time of the cells which become twice longer than usual cells, I tested at several times.

Fluorescence staining and microscopy

Logarithmically growing cells were fixed for 30 min in the growth medium supplemented with formaldehyde (final concentration; 3.7%) and potassium phosphate buffer (100 mM, pH 6.5) at 25 °C. Cells were sedimented by centrifugation and were further incubated in potassium phosphate buffer containing 4% formaldehyde for 45 min at room temperature. Actin staining was performed by overnight treatment with 20

U/ml Rhodamine-phalloidin (Molecular Probes, Inc., Eugene, OR, USA) in PBS. Then, the cells were washed three times with PBS and mixed with 20μg/ ml FITC-ConA (Sigma, St. Louis, MO, USA) in P buffer (10 mM sodium phosphate, 150 mM NaCl, pH 7.2) for 5 min to stain mannoprotein on the cell surface. After washing with P buffer twice, the cells were mixed with mounting buffer containing 20 μg/ml 4'-6'-diamidino-20phenylindole (DAPI, Sigma) for DNA staining and 1 μg/ ml p-phenylenediamine (Sigma) to inhibit fading. The specimens were observed with a Zeiss Axiophot2 imaging microscope (×100 objective). Images were captured using a cooled CCD camera CoolSNAPHQ (Roper Scientific Photometrics, Tucson, AZ, USA) interfaced with MetaMorph software (Universal Imaging Corporation, Downingtown, PA, USA).

Image processing program

Image-processing analysis with *CalMorph* (ver.1.0) was performed as described previously (Ohtani *et al.*, 2004). CalMorph is a program that can obtain a large amount of data as many morphological parameters automatically on cell cycle phase, cell forms, etc., for individual cells, from a set of pictures of cell walls, cell nuclei, and actins. CalMorph user manual is available at SCMD (http://scmd.gi.k.u-tokyo.ac.jp/datamine/).

Statistical analysis

The Mann–Whitney *U*-test was used to compare the drug-treated cells and control cells

at each concentration point examined. This non-parametric test compares two gropes that there is no correspondence in the data set. A value of $P < 0.001$ was considered significant.

Teardrop View

Teardrop View is a diagram consisting of rectangles whose positions and dimensions represent the values of a variable quantity. This data is obtained by Teardrop94 program being constructed to understand which morphological parameters of a particular mutant are abnormal (Saito *et al.*, 2005). This system displays the distribution of all mutants for each parameter and highlights the focal mutant value.

Gene ontology terms

The information of gene ontology annotations used in this study was published in *Saccharomyces* Genome Database (SGD) updated at 11th Dec. 2004 (Dwight *et al.*, 2002).

References

Ayscough KR, Stryker J, Pokala N, Sanders M, Crews P, Drubin DG. High rates of actin filament turnover in budding yeast and roles for actin in establishment and maintenance of cell polarity revealed using the actin inhibitor latrunculin-A. J Cell Biol. 1997 Apr 21;137(2):399-416.

Baetz K, McHardy L, Gable K, Tarling T, Reberioux D, Bryan J, Andersen RJ, Dunn T, Hieter P, Roberge M. Yeast genome-wide drug-induced haploinsufficiency screen to determine drug mode of action. Proc Natl Acad Sci U S A. 2004 Mar 30;101(13):4525-30.

Barlow T, Eliasson R, Platz A, Reichard P, Sjoberg BM. Enzymic modification of a tyrosine residue to a stable free radical in ribonucleotide reductase. Proc Natl Acad Sci U S A. 1983 Mar;80(6):1492-5.

Belmont LD, Patterson GM, Drubin DG. New actin mutants allow further characterization of the nucleotide binding cleft and drug binding sites. J Cell Sci. 1999 May;112 (Pt 9):1325-36

Dolma S, Lessnick SL, Hahn WC, Stockwell BR. Identification of genotype-selective antitumor agents using synthetic lethal chemical screening in engineered human tumor cells. Cancer Cell. 2003 Mar;3(3):285-96.

Dwight SS, Harris MA, Dolinski K, Ball CA, Binkley G, Christie KR, Fisk DG, Issel-Tarver L, Schroeder M, Sherlock G, Sethuraman A, Weng S, Botstein D, Cherry JM. Saccharomyces Genome Database (SGD) provides secondary gene annotation using the Gene Ontology (GO). Nucleic Acids Res. 2002 Jan 1;30(1):69-72.

Giaever G, Shoemaker DD, Jones TW, Liang H, Winzeler EA, Astromoff A, Davis RW. Genomic profiling of drug sensitivities via induced haploinsufficiency. Nat Genet. 1999 Mar;21(3):278-83.

Giaever G, Chu AM, Ni L, Connelly C, Riles L, Veronneau S, Dow S, Lucau-Danila A, Anderson K, Andre B, Arkin AP, Astromoff A, El-Bakkoury M, Bangham R, Benito R, Brachat S, Campanaro S, Curtiss M, Davis K, Deutschbauer A, Entian KD, Flaherty P, Foury F, Garfinkel DJ, Gerstein M, Gotte D, Guldener U, Hegemann JH, Hempel S, Herman Z, Jaramillo DF, Kelly DE, Kelly SL, Kotter P, LaBonte D, Lamb DC, Lan N, Liang H, Liao H, Liu L, Luo C, Lussier M, Mao R, Menard P, Ooi SL, Revuelta JL, Roberts CJ, Rose M, Ross-Macdonald P, Scherens B, Schimmack G, Shafer B, Shoemaker DD, Sookhai-Mahadeo S, Storms RK, Strathern JN, Valle G, Voet M, Volckaert G, Wang CY, Ward TR, Wilhelmy J, Winzeler EA, Yang Y, Yen G, Youngman E, Yu K, Bussey H, Boeke JD, Snyder M, Philippsen P, Davis RW, Johnston M. Functional profiling of the Saccharomyces cerevisiae genome. Nature. 2002 Jul 25;418(6896):387-91.

Giaever G, Flaherty P, Kumm J, Proctor M, Nislow C, Jaramillo DF, Chu AM, Jordan MI, Arkin AP, Davis RW. Chemogenomic profiling: identifying the functional interactions of small molecules in yeast. Proc Natl Acad Sci U S A. 2004 Jan 20;101(3):793-8

Goffeau A, Barrell BG, Bussey H, Davis RW, Dujon B, Feldmann H, Galibert F, Hoheisel JD, Jacq C, Johnston M, Louis EJ, Mewes HW, Murakami Y, Philippsen P, Tettelin H, Oliver SG. Life with 6000 genes. Science. 1996 Oct 25;274(5287):546, 563-7. Review.

Heitman J, Movva NR, Hall MN. Targets for cell cycle arrest by the immunosuppressant rapamycin in yeast. Science. 1991 Aug 23;253(5022):905-9.

Lashkari DA, DeRisi JL, McCusker JH, Namath AF, Gentile C, Hwang SY, Brown PO, Davis RW. Yeast microarrays for genome wide parallel genetic and gene expression analysis. Proc Natl Acad Sci U S A. 1997 Nov 25;94(24):13057-62.

Lum PY, Armour CD, Stepaniants SB, Cavet G, Wolf MK, Butler JS, Hinshaw JC,

Garnier P, Prestwich GD, Leonardson A, Garrett-Engele P, Rush CM, Bard M, Schimmack G, Phillips JW, Roberts CJ, Shoemaker DD. Discovering modes of action for therapeutic compounds using a genome-wide screen of yeast heterozygotes. Cell. 2004 Jan 9;116(1):121-37.

Marston AL, Tham WH, Shah H, Amon A. A genome-wide screen identifies genes required for centromeric cohesion. Science. 2004 Feb 27;303(5662):1367-70.

Morton WM, Ayscough KR, McLaughlin PJ. Latrunculin alters the actin-monomer subunit interface to prevent polymerization. Nat Cell Biol. 2000 Jun;2(6):376-8.

Ohtani M, Saka A, Sano F, Ohya Y, Morishita S. Development of image processing program for yeast cell morphology. J Bioinform Comput Biol. 2004 Jan;1(4):695-709.

Ohya Y, Sese J, Yukawa M, Sano F, Nakatani Y, Saito TL, Saka A, Fukuda T, Ishihara S, Oka S, Suzuki G, Watanabe M, Hirata A, Ohtani M, Sawai H, Fraysse N, Latge JP, Francois JM, Aebi M, Tanaka S, Muramatsu S, Araki H, Sonoike K, Nogami S, Morishita S. High-dimensional and large-scale phenotyping of yeast mutants. Proc Natl Acad Sci U S A. 2005 Dec 27;102(52):19015-20. Epub 2005 Dec 19.

Saito TL, Ohtani M, Sawai H, Sano F, Saka A, Watanabe D, Yukawa M, Ohya Y, Morishita S. SCMD: Saccharomyces cerevisiae Morphological Database. Nucleic Acids Res. 2004 Jan 1;32(Database issue):D319-22.

Saito TL, Sese J, Nakatani Y, Sano F, Yukawa M, Ohya Y, Morishita S. Data mining tools for the Saccharomyces cerevisiae morphological database. Nucleic Acids Res. 2005 Jul 1;33(Web Server issue):W753-7.

Shortle D, Haber JE, Botstein D. Lethal disruption of the yeast actin gene by integrative DNA transformation. Science. 1982 Jul 23;217(4557):371-3.

Shortle D, Novick P, Botstein D. Construction and genetic characterization of

temperature-sensitive mutant alleles of the yeast actin gene. Proc Natl Acad Sci U S A. 1984 Aug;81(15):4889-93.

Schreiber SL.Chemical genetics resulting from a passion for synthetic organic chemistry. Bioorg Med Chem. 1998 Aug;6(8):1127-52.

Tong AH, Evangelista M, Parsons AB, Xu H, Bader GD, Page N, Robinson M, Raghibizadeh S, Hogue CW, Bussey H, Andrews B, Tyers M, Boone C. Systematic genetic analysis with ordered arrays of yeast deletion mutants. Science. 2001 Dec 14;294(5550):2364-8.

Wertman KF, Drubin DG, Botstein D. Systematic mutational analysis of the yeast ACT1 gene. Genetics. 1992 Oct;132(2):337

Winzeler EA, Shoemaker DD, Astromoff A, Liang H, Anderson K, Andre B, Bangham R, Benito R, Boeke JD, Bussey H, Chu AM, Connelly C, Davis K, Dietrich F, Dow SW, El Bakkoury M, Foury F, Friend SH, Gentalen E, Giaever G, Hegemann JH, Jones T, Laub M, Liao H, Liebundguth N, Lockhart DJ, Lucau-Danila A, Lussier M, M'Rabet N, Menard P, Mittmann M, Pai C, Rebischung C, Revuelta JL, Riles L, Roberts CJ, Ross-MacDonald P, Scherens B, Snyder M, Sookhai-Mahadeo S, Storms RK, Veronneau S, Voet M, Volckaert G, Ward TR, Wysocki R, Yen GS, Yu K, Zimmermann K, Philippsen P, Johnston M, Davis RW. Functional characterization of the S. cerevisiae genome by gene deletion and parallel analysis. Science. 1999 Aug 6;285(5429):901-6.

Zewail A, Xie MW, Xing Y, Lin L, Zhang PF, Zou W, Saxe JP, Huang J. Novel functions of the phosphatidylinositol metabolic pathway discovered by a chemical genomics screen with wortmannin. Proc Natl Acad Sci U S A

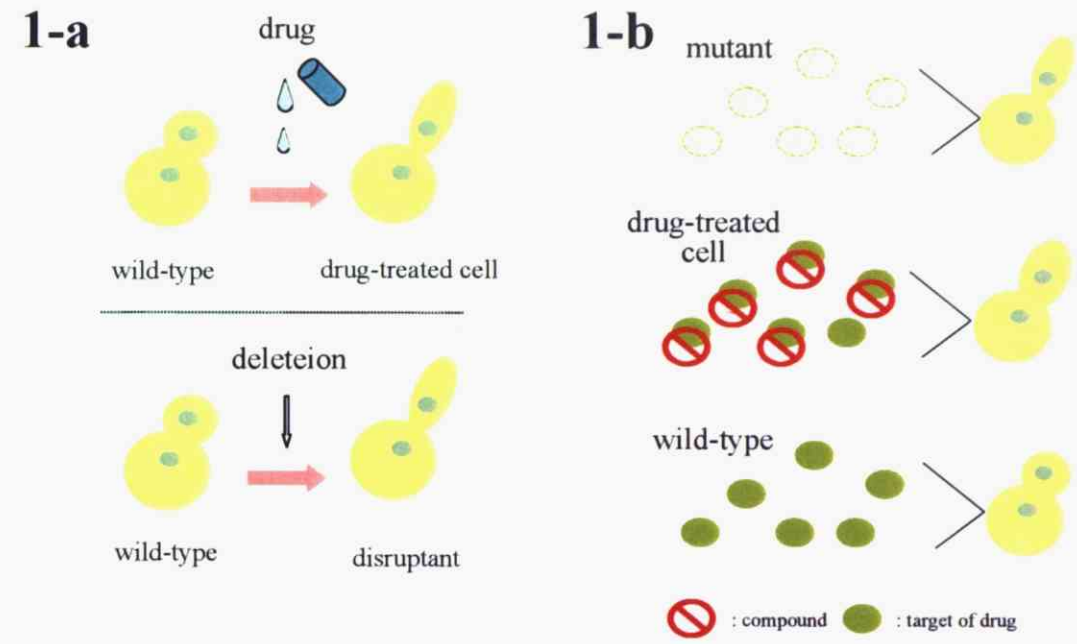

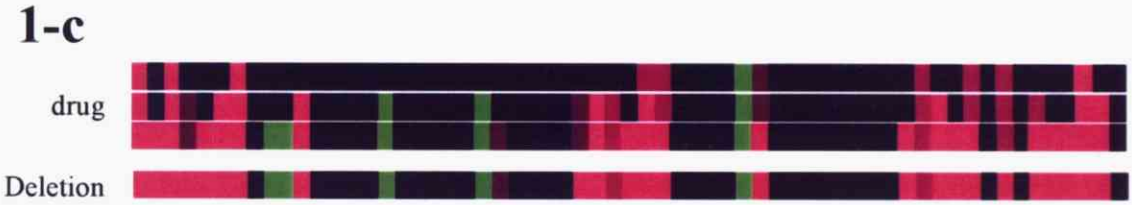

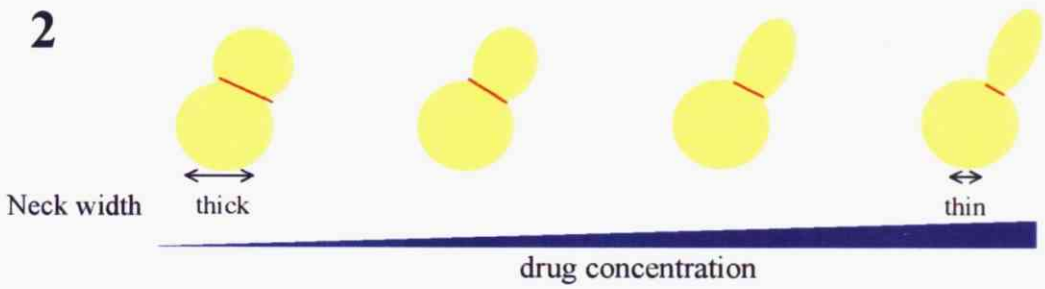

Figure 1 Premises for the novel strategy

Overview of the premises for discovering the drug target is shown.

Premise 1 The phenotype due to the drug-treatment is caused by impairment of the specific drug-target.

1-a) The phenotypic change induced by the drug resembles the one caused by impairment of the specific drug-target.

1-b) The phenotypic change caused by the gene deletion is more remarkable than the one by the drug-treatment.

1-c) Deletion of the drug target gene results in alteration in most of the phenotypic parameters that are affected by the drugs.

Premise 2 Drug concentration correlates with the values in the affected phenotypic parameters.

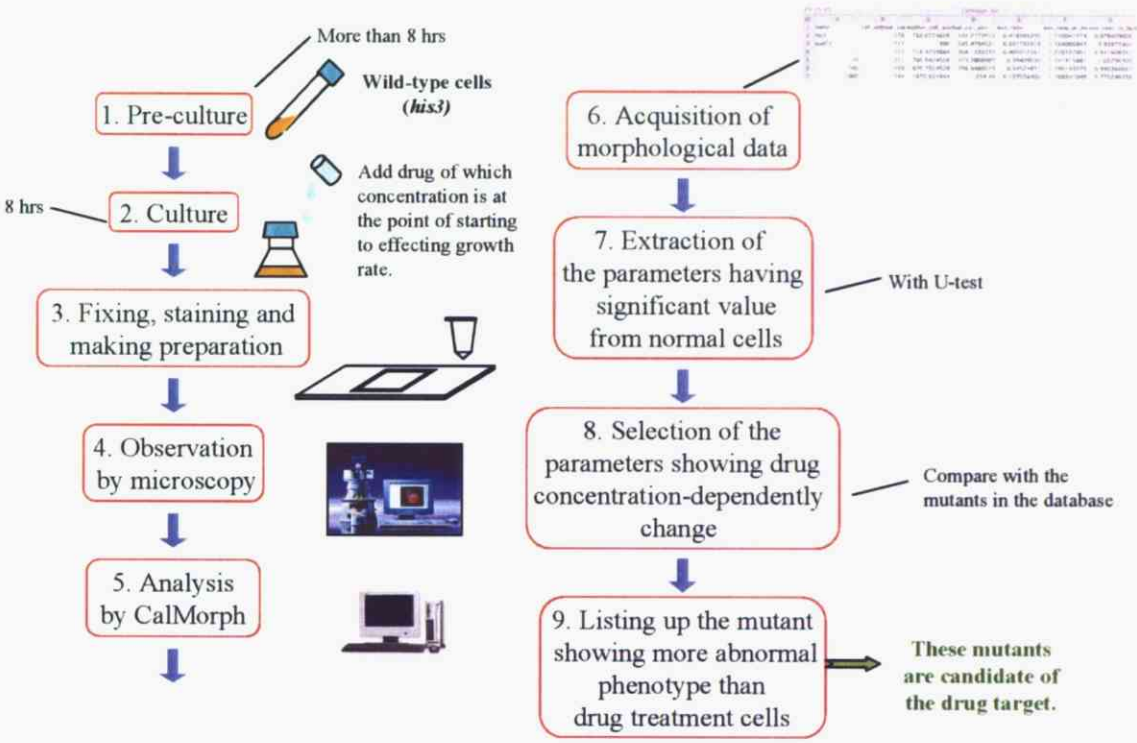

Figure 2 Systematic scheme of detecting target genes or proteins of drugs by chemical-genetic approaches

1) Pre-culture in YPD medium for more than 8 hrs.
2) Culture in the presence of drug for 8 hrs.
3) Fixation and staining the cells.
4) Microscopic observation of more than 200 cells.
5) Phenotypic analysis with CalMorph
6) Acquisition of morphological data.
7) Extraction of the parameters having significant valure from normal cells with U-test.
8) Selection of the parameters showing drug concentration-dependently change
9) Listing up the mutant showing more abnormal phenotype than drug treatment cells.

a

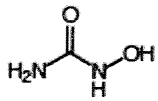

b

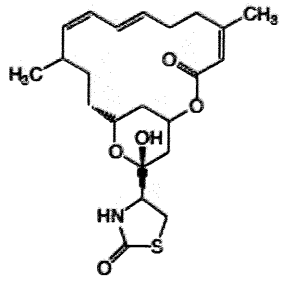

Figure 3 Chemical structures of compounds in this study

a. Hydroxyurea: HU inhibits dNTP synthesis and can be particularly toxic to cells lacking S phase checkpoints (since they fail to respond to slow progression of replication) and to cells with impaired replication.

b. Latrunculin A: LAT-A binds to actin monomers and inhibits actin polymerization.

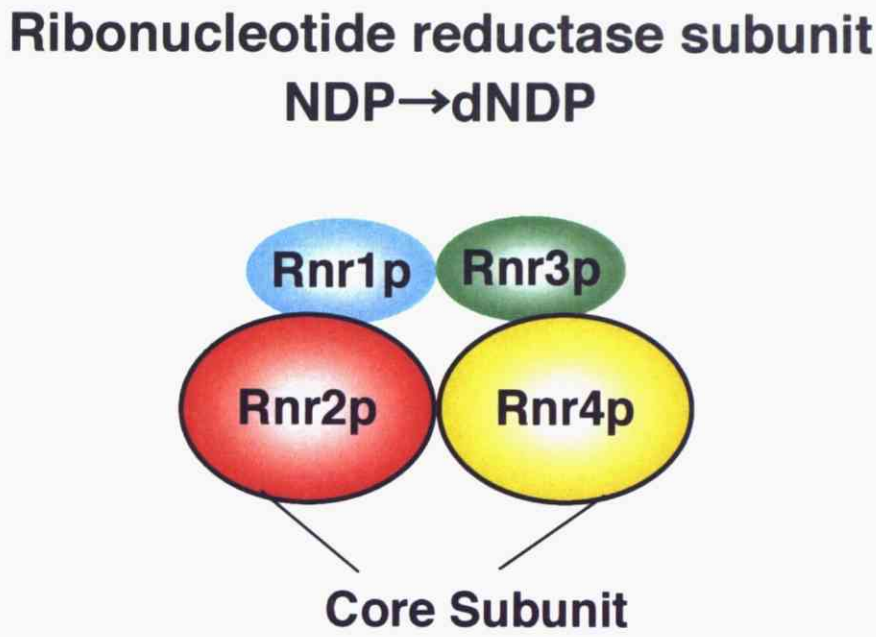

Figure 4 The model of ribonucleotide reductase subunit
RNR1 and *RNR3* encode alpha subunits and *RNR2* and *RNR4* encode beta subunits. Rnr2p has dNDP catalysis domein. Ribonucleotide reductase catalysis conversion of ribonucleoside diphosphates to the corresponding deoxyribonucleotides to provideabalanced supply of precursors for DNA synthesis.

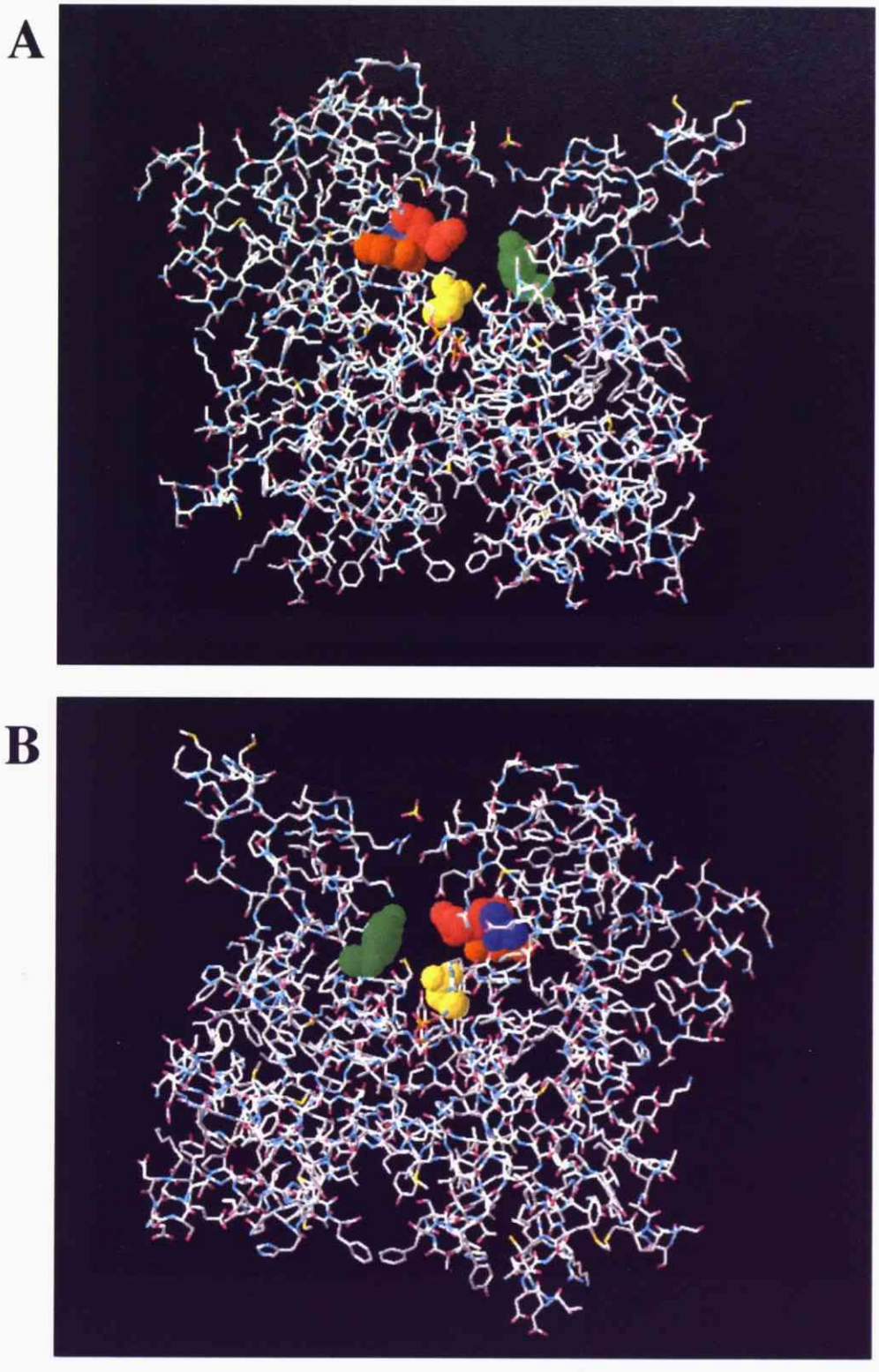

Figure 5 Location on the surface of actin of mutants conferring resistance to Lat-A
Front (A) and back (B) views of space-filling model of yeast actin.
The location of amino acids mutated in all of the Lat-A resistant mutations identified.
Blue: T186, Green: Y69, Orange: E214, Pink: R210, Yellow: D157

A

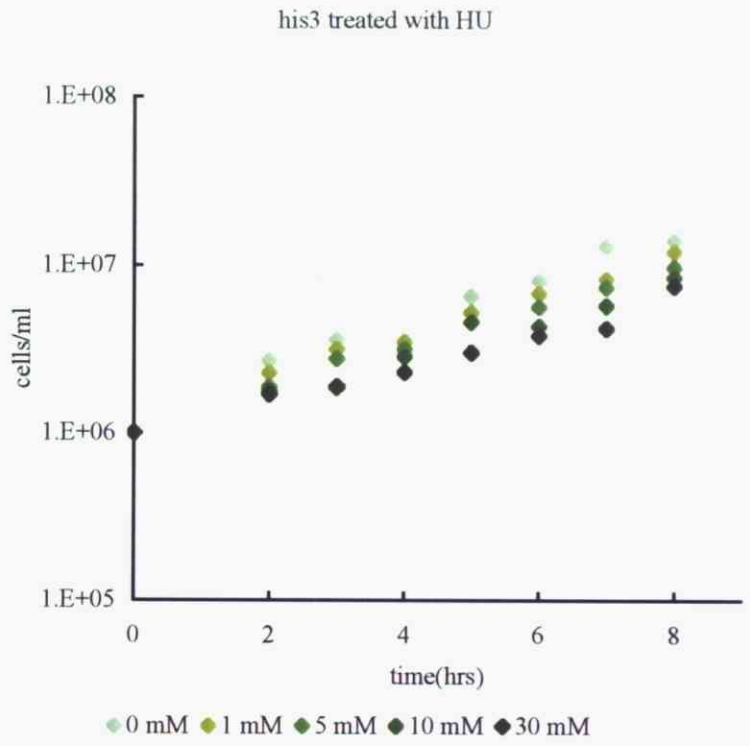

B

concentration	doubling time (h)	ratio
0 mM	2.02	1.00
5 mM	2.34	1.16
10 mM	2.48	1.23
20 mM	3.03	1.50
30 mM	3.94	1.95

Figure 6 Growth curve of cells that cultured in YPD containing HU
Cells from overnight cultures were inoculated on fresh YPD containing drug. **A**: Number of cells was counted and plotted against drug concentrations. **B**: The doubling time is getting longer in HU-concentration manner. It indicates the growth that was affected by HU.

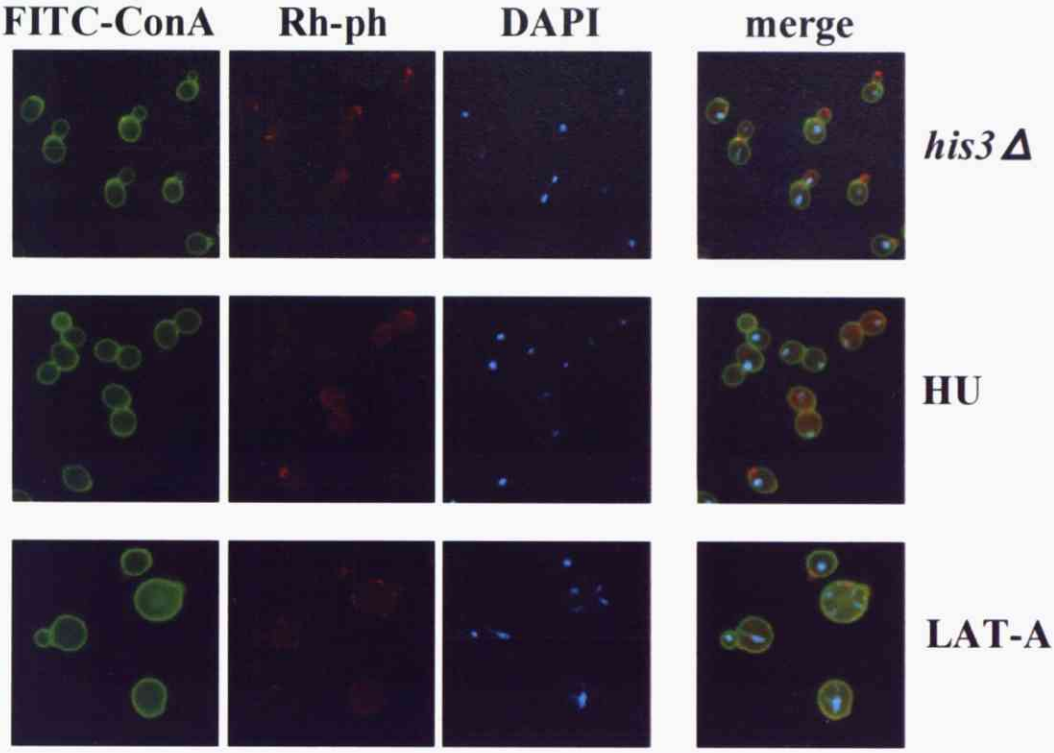

Figure 7 Triple stained images of the drug-treated cells for quantitative presentation
Each cell was grown in YPD medium with drug (HU: 30 mM HU, LAT-A: 1.5 μM) or DMSO (*his3Δ*), and log-phase cells were fixed. To obtain fluorescent images of cell wall, actin cytoskeleton and nuclear DNA, cells were triply stained with FITC-concanavalin A (FITC-conA), rhodamine-phalloidin (Rh-ph) and DAPI, respectively.

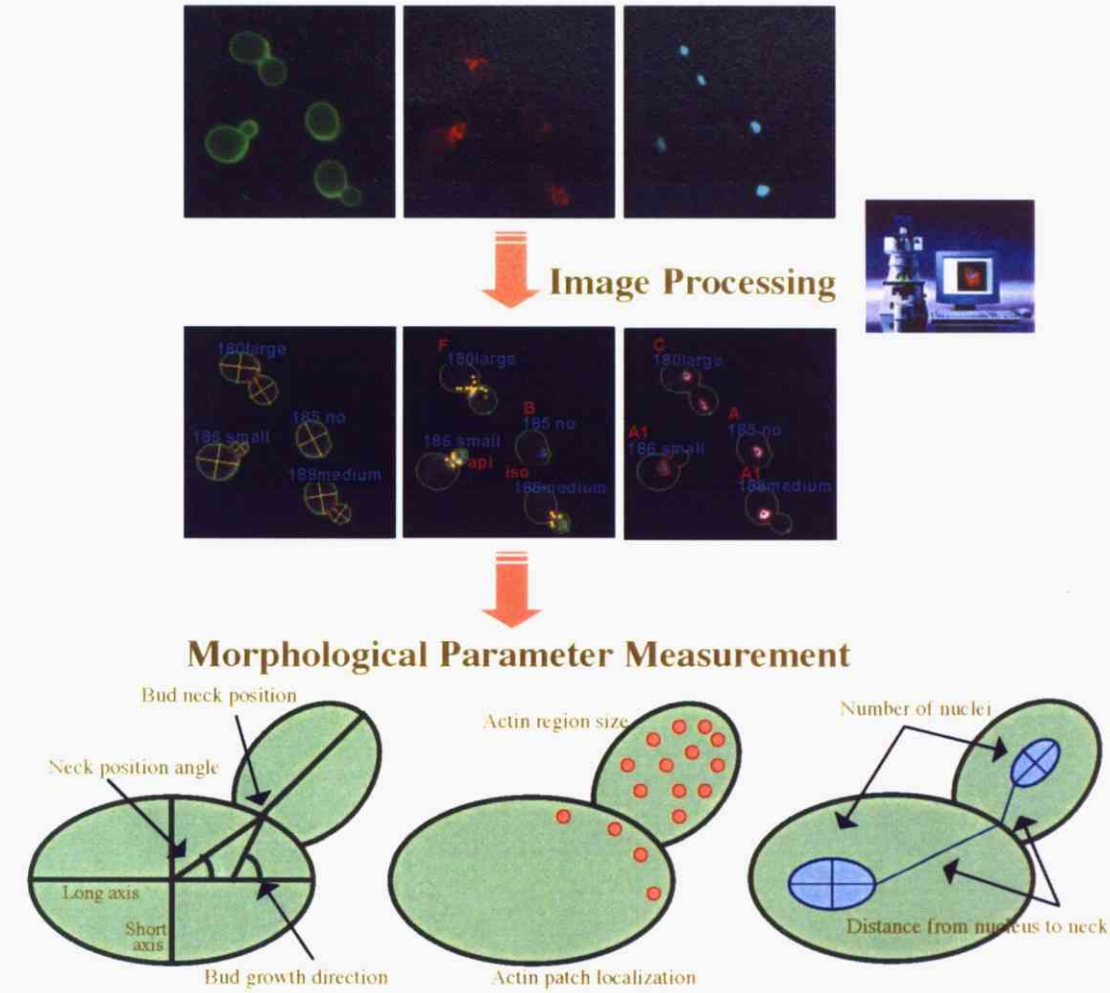

Figure 8 The scheme of the image processing program CalMorph
Input photos of cells strained with FITC–ConA, DAPI and Rh-ph to visualize the cell wall, nuclei and actin distribution, respectively. The images are automatically recognized and described in the form of Excel data sheets by the image-processing program CalMorph. Several examples of 500 morphological parameters are descrived. These morphological parameter are used for detailed analysis of the morphology.

High Correlation

Low Correlation

correlation coefficient = 0.98

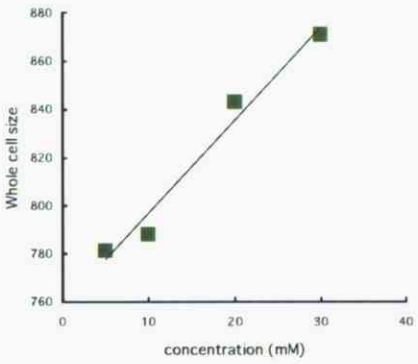

C11-1_A, C12-1_A, C103_A, C104_A, D102_A, D117_A, D127_A, D135_A, C11-2_A1B, C101_A1B, C102_A1B, C108_A1B, C111_A1B, C113_A1B, D104_A1B, D126_A1B, D142_A1B, D145_A1B, D200, D207, D209, D211, D214, D216 (24 parameters)

correlation coefficient = -0.11

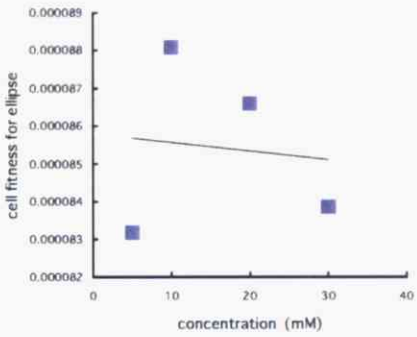

C13_A (1 parameter)

Figure 9 The list of the parameters showing concentration of HU dependent change

The left 24 parameters have the high correlation coefficient ($R > 0.8$) with HU. It indicated these parameters reflected drug effects. The right parameter has the low correlation coefficient ($R < 0.8$) with HU concentration. The parameters in bold is a representative of each scatter plot.

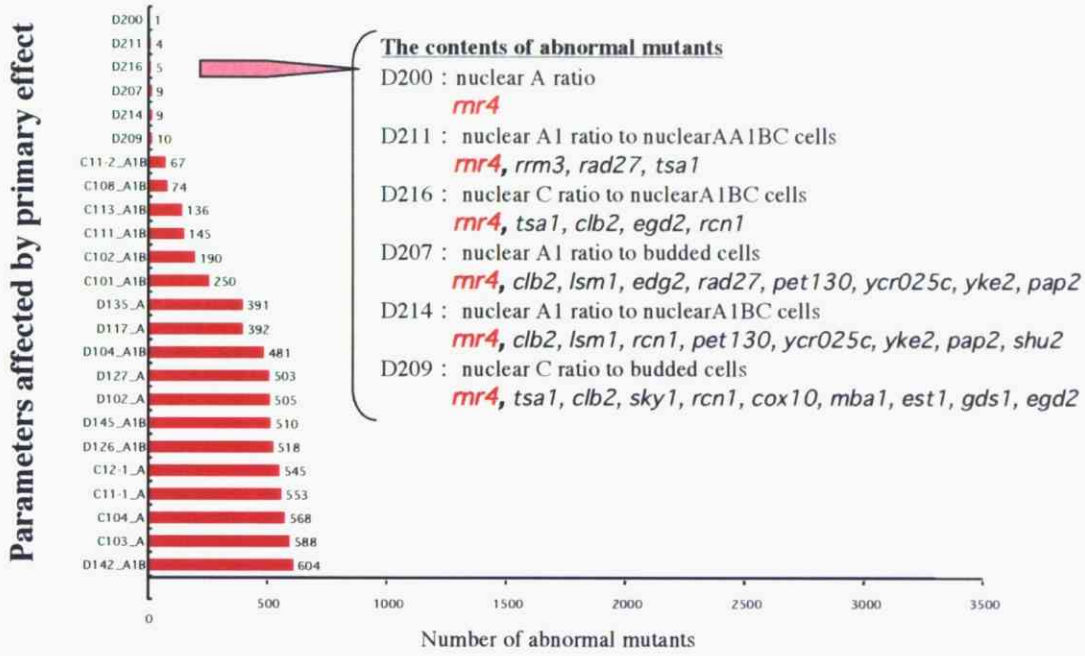

Figure 10 The numbers of the mutant have abnormal phenotype in the significant parameters of HU
The numbers next to the bar graph indicate the total number of the mutants that show more abnormal morphology than the phenotype of the cells treated with 30 mM HU. Some of the abnormal mutants in representative parameters are shown in the out of the graph.

A

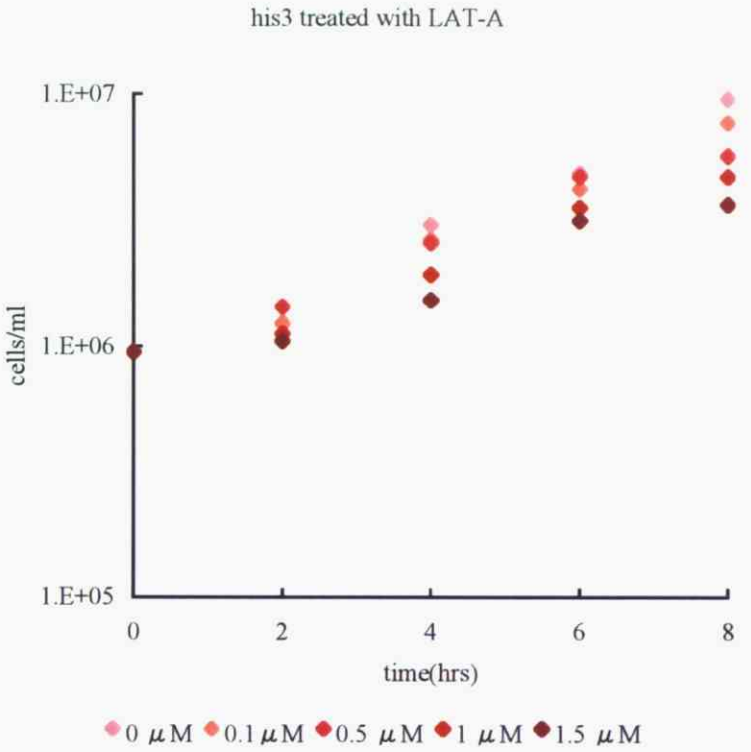

B

concentration	doubling time (h)	ratio
0 μM	2.31	1.00
0.1 μM	2.56	1.11
0.5 μM	2.90	1.26
1 μM	3.18	1.38
1.5 μM	3.65	1.58

Figure 11 Growth curve of cells that cultured in YPD containing LAT-A
Cells from overnight cultures were inoculated on fresh YPD containing LAT-A. **A**: Number of cells was counted and plotted against drug concentrations. **B**: The doubling time is getting longer in LAT-A-concentration manner. It indicates the growth that was affected by LAT-A.

High Correlation

correlation coefficient = 0.99

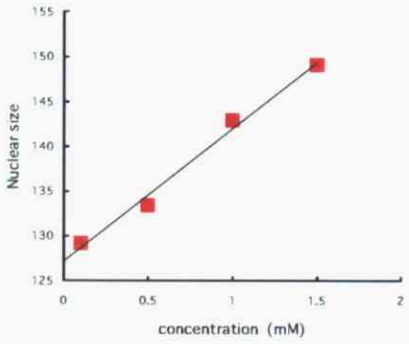

CCV12-2_A1B, CCV109_A1B, DCV152_A1B, **D14-3_C**, DCV14-1_C, DCV108_C, D203, D206 (8 parameters)

Low Correlation

correlation coefficient = -0.19

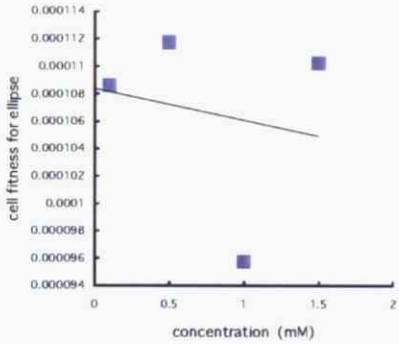

C13_A, CCV126_A, D196_A1B, CCV107_A1B, CCV117_A1B, CCV118_A1B, D14-2_C, D157_C, D174_C, D189_C, D195_C, DCV117_C, DCV135_C, DCV145_C, DCV147_C, DCV148_C, DCV150_C, DCV163_C, DCV166_C, DCV167_C (20 parameters)

Figure 12 The list of the parameters showing concentration of LAT-A dependent change

The left 8 parameters have the high correlation coefficient ($R > 0.8$) with LAT-A. It indicated these parameters reflected drug effects. The right parameters have the low correlation coefficient ($R < 0.8$) with LAT-A concentration. The parameters in bold is a representative of each scatter plot.

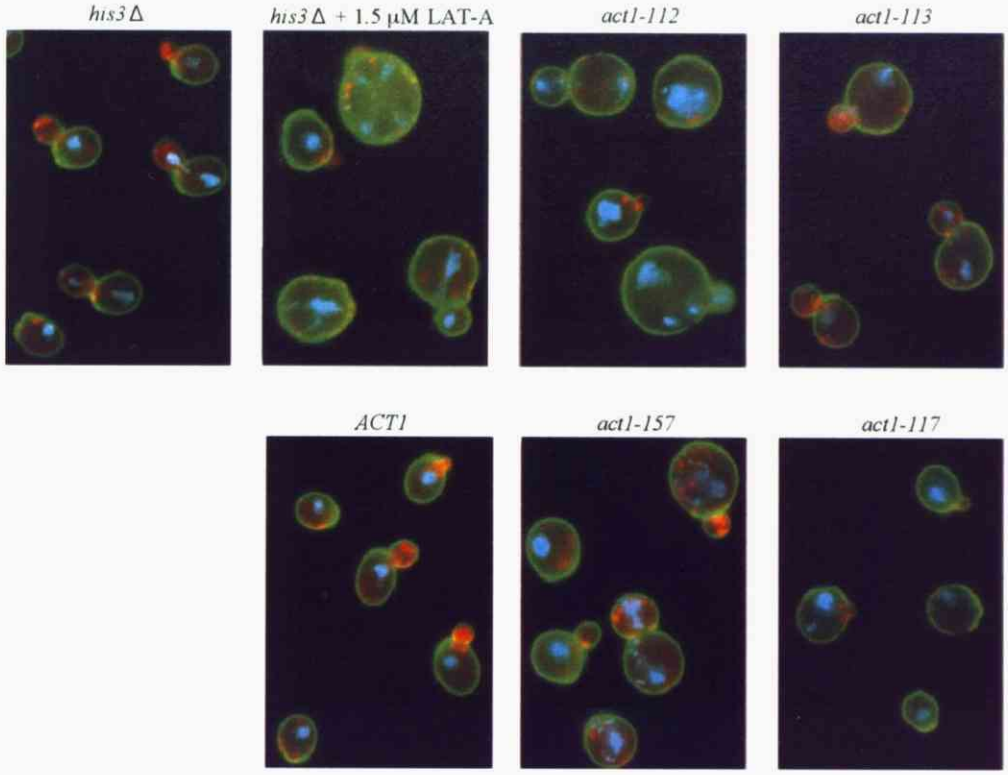

Figure 13 Triple stained images of the *ACT1* alleles and LAT-A-treated cells for quantitative presentation

his3Δ+1.5 μM LAT-A: his3 was cultured in YPD containing 1.5μM LAT-A for 8 hrs. The other cells were cultured in fresh YPD medium for 8 hrs. Each log-phase cell was fixed. To obtain fluorescent images of cell wall, actin cytoskeleton and nuclear DNA, cells were triply stained with FITC-concanavalin A (FITC-conA), rhodamine-phalloidin (Rh-ph) and DAPI, respectively. The genetic backgrounds of *ACT1, act1-112, act1-113, act1-117 and act1-157* are different from BY strain (*his3Δ*). To compare these morphology, The data of ACT1 alleles were normalized by *his3Δ*.

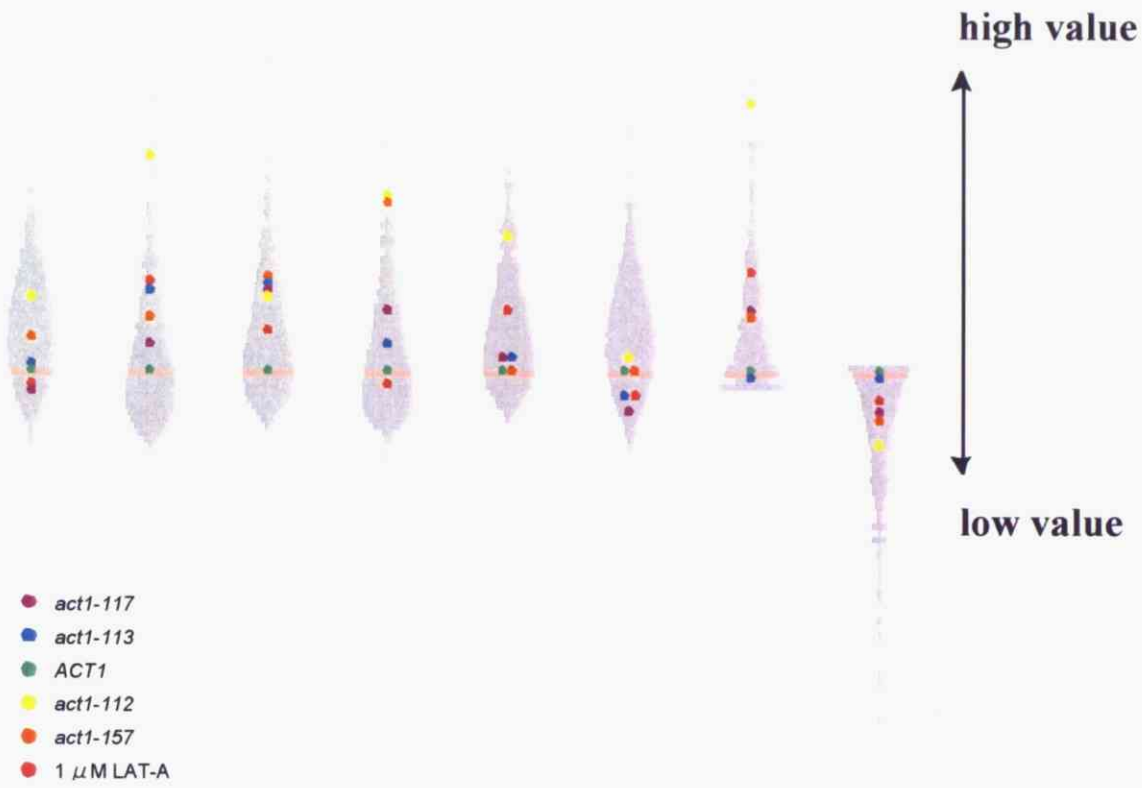

Figure 14 Distributions of all mutants, allele of *ACT1* mutants and 1.5 μM LAT-A treated cells in the significant parameter

Teardrop View is the distribution of all mutants for each parameter and highlights the focal mutant value. Dots indicate the morphological parameter distributions of each strain.Light pink bars indicate the value of *his3* (YOR202w). The value of *ACT1* mutants are normalized by the value of *his3*.

A

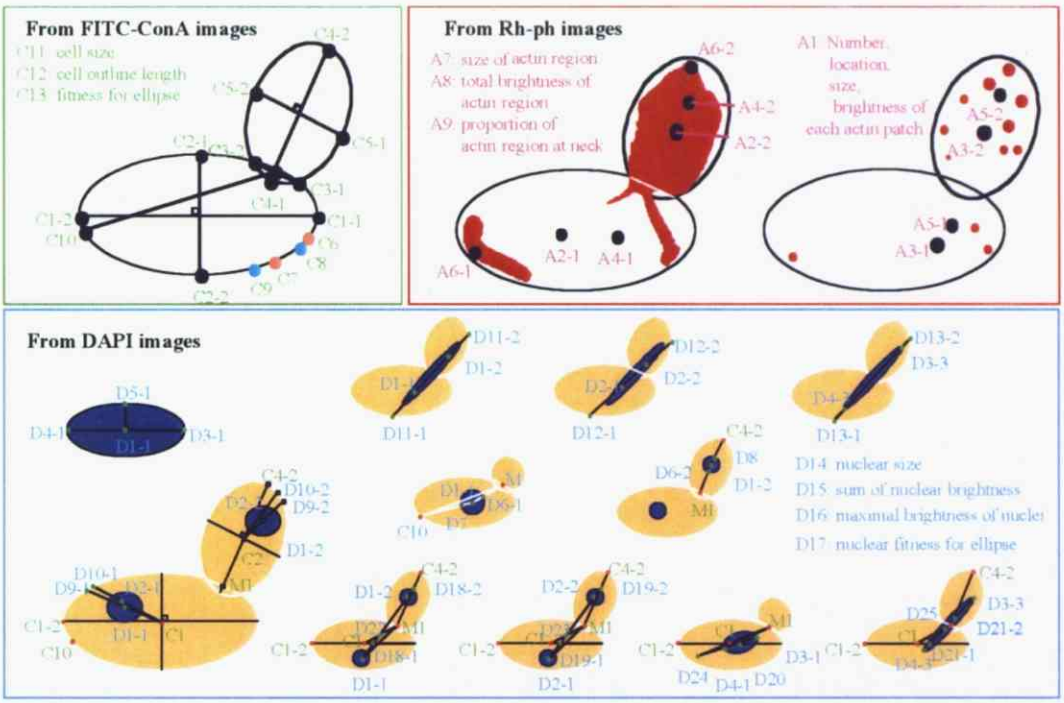

B

D_group: classification based on nuclear number and position

A	No_bud_cells_with_one_nucleus
A1	Budded_cells_with_one_nucleus_in_the_mother_cell
B	Budded_cells_in_which_the_nucleus_is_dividing_at_the_neck
C	Budded_cells_with_one_nucleus_each_in_the_mother_cell_and_bud
D	No_bud_cells_with_two_nuclei_or_budded_cells_with_two_nuclei_together_in_either_the_mother_cell_or_bud
E	Cells_with_no_nucleus_or_with_more_than_two_nuclei
F	Budded_cells_with_one_nucleus_only_in_the bud

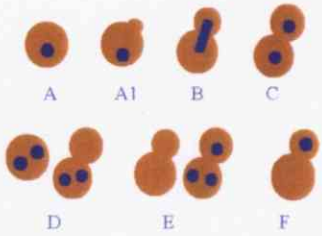

Figure 15 Established 94 basic parameters extracted from FITC-ConA, Rh-ph and DAPI images.

The 501 biological parameter calculated from these basic parameters.

(A) Description of 94 Basic parameters are the ones extracted directly from the images.

(B) Data items based on nuclear number and position.

Table 1 List of yeast strains used in this study

	strain	Genotype	
BY4741	*his3*	a *his3 Δ 1 leu2 Δ 0 met15 Δ 0 ura3 Δ 0*	a
DDY354	*ACT1*	a *ACT1::HIS3, cry1*	b
DDY355	*act1-112*	a *act1-112::HIS3, ade2-101, ade4, cry1*	b
DDY342	*act1-113*	a *act1-113::HIS3, can1-1*	b
DDY345	*act1-117*	a *act1-112::HIS3, ade2-101, cry1*	b
DDY1537	*ACT1/act1-157*	a/ α *ACT1/act1-157::HIS3, ade2-101/ADE2, ADE4/ade4, cry1/CRY1*	b
	act1-157	a *act1-157::HIS3, ade2-101, ade4, cry1*	c

a: EUROSCARF
b: Wertman *et al.*
c: this study

Table 2 Oligonucleotides used in this study

name	sequence 5'-3'	souce
OK/arf1-check-F	AGAAAAACCATGTTATTACCCTTCC	this study
OK/asf1-check-F	AATGCTGTTTTATTCCGTTCTTACA	this study
OK/bud14-check-F	AAGCTTCTACAGGGGTACGCTGGT	this study
OK/cap1-check-F	TTGTTTCCTTTCCAACTATTTTTC	this study
OK/cap2-check-F	TTCTTTCTTCTTCCTTCAACGTCTA	this study
OK/cax4-check-F	TTCTTTATGCTTTTAATTACGCCAG	this study
OK/chs6-check-F	TAATAAAACAGTGATAGCAGAGCGG	this study
OK/cik1-check-F	CACTGTCGTAGCTCGTATCAAAATA	this study
OK/clc1-check-F	GTTAATCCAGTAAGCGGAACAAGTA	this study
OK/clc1-check-R	TGGATCCAACAAGTAAAATGAAAAT	this study
OK/ctf18-check-F	TACTGTAACCATTGTGTTTTAGGGC	this study
OK/cwh36-check-F	TGTTTTGTGCAGTGTATTACCAACT	this study
OK/cyk3-check-F	AACAAGAGAAAAGGCCAAAATTAAC	this study
OK/dcc1-check-F	GGCAGCGTATAGTATAACCAGAAAA	this study
OK/dia2-check-F	CTGCGTTCGTAGTAAAATCAGAAAT	this study
OK/end3-check-F	TAACATCAAGTTCCTTGAACAAACA	this study
OK/erd1-check-F	GTCCGCTTGGTAAAAGTCAGTAATA	this study
OK/esc1-check-F	AGGAATTTAAAATGCGAGAAAGTCT	this study
OK/est1-check-F	AAACTGCCTTCGCTATAGAATTTT	this study
OK/est2-check-F	TTAGTTTGGGCGTATTTACATCTTT	this study
OK/est3-check-F	AATTTTCATAGAAACAAATCCGTGA	this study
OK/gas1-check-F	AAAAAGAAAAGTCGGGAAAATAATG	this study
OK/gup1-check-F	ATCAGCTCAATCGGACATAAAAATA	this study
OK/hex3-check-F	TCTCTTTATCCTTGGATTGAATCTG	this study
OK/hnt3-check-F	AGAATTAGGAGAAACTTTGACGGAT	this study
OK/kin3-check-F	GGCACAGTCTTCCGATAGTTACAGC	this study
OK/mdm20-check-F	AGTTCTTTGCTTGTTCATAAATTGC	this study
OK/med2-check-F	GAATTGGTACCTTTTAGTTGTGCAT	this study
OK/mms1-check-F	CTAAATTTGGAAACATGAGAAAGGA	this study
OK/MMS22-check-F	AGAAGCAGTTCTTTTAATCTTTGGG	this study
OK/mre11-check-F	GTTCACAAGCAAGCCTGTAAATAAT	this study
OK/mrm2-check-F	ACCATCTTCATGTATCGTTTTTGAT	this study
OK/myo5-check-F	AAACTAATGACGGCTAAAATTAAGTCA	this study
OK/nfi1-check-F	TGTTCAACAAAATGTGATAAAGGAA	this study
OK/npy1-check-F	TTTTATATATTTTGCCACATCGCTT	this study
OK/nsr1-check-F	TTTTGGATAAAGCAATTGAAGAAAG	this study

OK/pmr1-check-F	CCCTAGATAACCACTTAACAGCAAA	this study
OK/pol32-check-F	AATTCTCGATCAGTATGCCTCAATA	this study
OK/prs3-check-F	GCTCATCGATTTTTCTTTTCTTTTT	this study
OK/rad18-check-F	GGGCTGGAGTTATCATATCACATAG	this study
OK/rad50-check-F	ATAACCATGCATCTTGCAATACTTT	this study
OK/rad51-check-F	CCAATCTAGTTTAGCTATCCTGCAA	this study
OK/rad54-check-F	TAAAAAGTATTTTACGCGTTACCCA	this study
OK/rcr1-check-F	AGAGGGAGAAGAACATAATTCGTTT	this study
OK/RPL12B-check-F	TCCGTTTGCGTGACTTTATACTAAT	this study
OK/rtt107-check-F	ACTTAACCACAGAATGTTCTTCGAC	this study
OK/sac3-check-F	AGAATTCGTGATTCAATGTTCATTAT	this study
OK/scp160-check-F	CTCTTAAAGACTTGCAACGGATAGT	this study
OK/spt10-check-F	TACCACTTTTAAGTTTTTGGTCAGG	this study
OK/swa2-check-F	AACAAGTGCAGGCTAACATACTTTC	this study
OK/tpm1-check-F	AAGAACTTAAAAAGACAAACCAGCC	this study
OK/ubc4-check-F	ATTGTTATAGTTTTTCTCGAAGCGA	this study
OK/vps15-check-F	AGACAGTACCATTGGAAAACTTGAG	this study
OK/vps16-check-F	ATTTCTGACAAAAGCAAACAATAGG	this study
OK/vps64-check-F	GCACATTTTAAAGACTCCACAGAAT	this study
OK/yal058c-a-check-F	GCGAAAATAGAAAGATAATTCGTCA	this study
OK/ydl032w-check-F	GTGGAGTTGATTTGTGAAAGGTAAT	this study
OK/ygl024w-check-F	GAGTGGTTGGTGCTTACAACAGT	this study
OK/ygl217c-check-F	TAGTTCCTCCATGGCTAGAAATATG	this study
OK/ylr338w-check-F	GTAGTATTTGGTAACGGTGGTGCTA	this study
OK/yml053c-check-F	CTGGGTAACCGATTTTTCTCTCCCT	this study
OK/ynl086w-check-F	GAGTATGTGTCACGAAATCATCTTG	this study
OK/ynl171c-check-F	CTGCTACCAGGCAGTATATGAGAAT	this study
OK/yol008w-check-F	CAGTGTTATAGCAGGACCAACTTTT	this study
AI/KanB	TGTACGGGCGACAGTCACAT	A

Reference: A; Ikenishi unbublished

Table 3 Morphological parameters used in this study

ID	Description	Definition
C11-1_A	Whole_cell_size	-
C12-1_A	Whole_cell_outline_length	-
C13_A	Whole_cell_fitness_for_ellipse	-
C103_A	Long_axis_length_in_whole_cell	C1-1C1-2*
C104_A	Short_axis_length_in_whole_cell	C2-1C2-2
C126_A	Brightness_difference_of_cell_wall	C6-C7
D102_A	Distance_between_nuclear_gravity_center_and_mother_tip	D1-1C1-1 or D1-1C1-2
D117_A	Distance_between_nuclear_gravity_center_and_cell_center	D1-1C1
D127_A	Distance_between_nuclear_brightest_point_and_cell_tip	D2-1C1-1 or D2-1C1-2
D135_A	Distance_between_nuclear_brightest_point_and_cell_center	D2-1C1
CCV126_A	Coefficient_of_variation_of_C126_A	-
C11-2_A1B	Bud_cell_size	-
C12-2_A1B	Bud_cell_outline_length	-
C101_A1B	Whole_cell_size	C11-1+C11-2
C102_A1B	Whole_cell_outline_length	C12-1+C12-2
C107_A1B	Long_axis_length_in_bud	C4-1C4-2
C108_A1B	Short_axis_length_in_bud	C5-1C5-2
C109_A1B	Neck_width	C3-1C3-2
C111_A1B	Distance_between_bud_tip_and_mother_short_axis_extension	-
C113_A1B	Distance_between_bud_tip_and_mother_long_axis_through_middle_point_of_neck	C2C4-1
C117_A1B	Cell_outline_ratio	C12-1/C12-2
C118_A1B	Cell_size_ratio	C11-2/C11-1
D104_A1B	Distance_between_nuclear_gravity_center_and_mother_tip	D1-1C1-2
D126_A1B	Distance_between_nuclear_gravity_center_and_mother_hip	D1-1C10
D142_A1B	Distance_between_nuclear_brightest_point_and_mother_hip	D2-1C10
D145_A1B	Distance_between_nuclear_outline_point_D7_and_mother_hip	D7C10
D152_A1B	Mobility_of_nucleus_in_mother	D6-1C4-1/D7C10
D196_A1B	Maximal_intensity_of_nuclear_brightness_divided_by_average	D16-3/(D15-3/D14-3)
CCV12-2_A1B	Coefficient_of_variation_of_C12-2_A1B	-
CCV107_A1B	Coefficient_of_variation_of_C107_A1B	-
CCV109_A1B	Coefficient_of_variation_of_C109_A1B	-
CCV117_A1B	Coefficient_of_variation_of_C117_A1B	-
CCV118_A1B	Coefficient_of_variation_of_C118_A1B	-
DCV152_A1B	Coefficient_of_variation_of_D152_A1B	-

D14-1_C	Nuclear_size_in_mother	-
D14-2_C	Nuclear_size_in_bud	-
D108_C	Distance_between_nuclear_gravity_center_in_mother_and_middle_point_of_neck	D1-1C4-1
D117_C	Distance_between_nuclear_gravity_center_in_mother_and_mother_center	D1-1C1
D135_C	Distance_between_nuclear_brightest_point_in_mother_and_mother_center	D2-1C1
D143_C	Distance_between_nuclear_outline_point_D6-1_in_mother_and_middle_point_of_neck	D6-1C4-1
D145_C	Distance_between_nuclear_outline_point_D7_in_mother_and_mother_hip	D7C10
D147_C	Relative_distance_of_nuclear_gravity_center_in_mother_to_mother_center	D1-1C1/C1D9-1
D148_C	Relative_distance_of_nuclear_brightest_point_in_mother_to_mother_center	D2-1C1/C1D10-1
D150_C	Relative_distance_of_nuclear_brightest_point_in_bud_to_bud_center	D2-2C2/C2D10-2
D157_C	Angle_between_C2D2-2_and_C2C4-2	∠D2-2C2C4-2
D163_C	Angle_between_D2-1D2-2_and_C1C4-1	Angle_between_D2-1D2-2_and_C1C4-1
D166_C	Angle_between_D1-1D1-2_and_C4-1C4-2	Angle_between_D1-1D1-2_and_C4-1C4-2
D167_C	Angle_between_D2-1D2-2_and_C4-1C4-2	Angle_between_D2-1D2-2_and_C4-1C4-2
D174_C	Maximal_distance_between_nuclear_gravity_center_and_nuclear_outline_in_bud	D1-2D3-2
D189_C	Distance_between_nuclear_gravity_center_and_brightest_point_in_bud	D1-2D2-2
D195_C	Maximal_intensity_of_nuclear_brightness_divided_by_average_in_mother	D16-2/(D15-2/D14-2)
DCV14-1_C	Coefficient_of_variation_of_D14-1_C	-
DCV108_C	Coefficient_of_variation_of_D108_C	-
DCV117_C	Coefficient_of_variation_of_D117_C	-
DCV135_C	Coefficient_of_variation_of_D135_C	-
DCV145_C	Coefficient_of_variation_of_D145_C	-
DCV147_C	Coefficient_of_variation_of_D147_C	-
DCV148_C	Coefficient_of_variation_of_D148_C	-
DCV150_C	Coefficient_of_variation_of_D150_C	-
DCV163_C	Coefficient_of_variation_of_D163_C	-
DCV166_C	Coefficient_of_variation_of_D166_C	-
DCV167_C	Coefficient_of_variation_of_D167_C	-
D200	nuclear_A1_ratio	-
D203	nuclear_D_ratio	-
D207	nuclear_A1_ratio_to_budded_cells	-
D209	nuclear_C_ratio_to_budded_cells	-
D211	nuclear_A1_ratio_to_nuclear_AA1BC_cells	-
D214	nuclear_A1_ratio_to_nuclear_A1BC_cells	-
D216	nuclear_C_ratio_to_nuclear_A1BC_cells	-

*: The basic parameters descrived in Figure 14.

Table 4 List of the mutants that show more abnormal phenotype than the HU-treated cells

Systematic Name	gene name	Molecluer Function	The number of the parameter*
YGR180C	*rnr4*	ribonucleoside-diphosphate reductase activity	24
YHR031C	*rrm3*	ATP-dependent DNA helicase activity, DNA helicase activity	19
YKL113C	*rad27*	5'-flap endonuclease activity	18
YLR233C	est1	RNA binding, single-stranded DNA binding, telomerase activity	18
YJL023C	*pet130*	unknown	18
YOL115W	*pap2*	DNA-directed DNA polymerase activity, polynucleotide adenylyltransferase activity	18
YHR193C	*egd2*	unfolded protein binding	14
YCR025C	YCR025C	unknown	13
YML028W	*tsa1*	thioredoxin peroxidase activity	12

*: The number of parameters where each mutant scored more abnormal value than drug-treated cells.

Table 5 List of the mutants that show more abnormal phenotype than the LAT-A-treated cells

Systematic Name	gene name	Biological Process	A*	B**
YEL036C	*anp1*	protein amino acid N-linked glycosylation	7	79
act1-112		alleles of ACT1(K213A, E214A, K215A)	6	
YBR200W	*bem1*	cellular morphogenesis during conjugation with cellular fusion, establishment of cell polarity (sensu Fungi)		49
YDL116W	*nup84*	DNA metabolism		66
YEL044W	*ies6*	metabolism		74
YKL113C	*rad27*	DNA repair, DNA replication		79
YML112W	*ctk3*	protein amino acid phosphorylation, regulation of transcription from RNA polymerase II promoter		45
YMR060C	*sam37*	outer mitochondrial membrane organization and biogenesis		4
YMR116C	*asc1*	negative regulation of transla		63
YOL072W	*thp1*	DNA recombination, bud site selection		41
YOR080W	*dia2*	invasive growth (sensu Saccharomyces), protein ubiquitination		102
YAL035W	*fun12*	translational initiation	5	20
YAL047C	*spc72*	microtubule nucleation, nuclear migration, microtubule-mediated		68
YBL025W	*rrn10*	transcription from RNA polymerase I promoter		63
YBL058W	*shp1*	glycogen metabolism, proteasomal ubiquitin-dependent protein catabolism		66
YBL062W		biological process unknown		12
YBL094C		biological process unknown		86
YBR194W	*soy1*	biological process unknown		50
YCL036W	*gfd2*	biological process unknown		0
YDR138W	*hpr1*	biological process unknown		78
YDR433W		biological process unknown		24
YDR442W		biological process unknown		32
YFR019W	*fab1*	phospholipid metabolism, vacuole organization and biogenesis		23
YGL070C	*rpb9*	transcription from RNA polymerase II promoter		52
YGR006W	*prp18*	formation of catalytic spliceosome for second transesterification step, nuclear mRNA splicing, via spliceosome		59
YJL080C	*scp160*	chromosome segregation, intracellular mRNA localization		85

YJL127C	*spt10*	chromatin remodeling, regulation of global transcription from RNA polymerase II promoter	83
YJL204C	*rcy1*	endocytosis	39
YKL054C	*def1*	response to DNA damage stimulus, telomere maintenance,ubiquitin-dependent protein catabolism	55
YKL139W	*ctk1*	protein amino acid phosphorylation, regulation of transcription from RNA polymerase II promoter	61
YLR447C	*vma6*	vacuolar acidification, vacuolar transport	32
YMR091C	*npl6*	protein import into nucleus	50
YNL139C	*rlr1*	DNA recombination, RNA elongation from RNA polymerase II promoter, mRNA export from nucleus	60
YNL206C	*rtt106*	negative regulation of DNA transposition	28
YNL250W	*rad50*	double-strand break repair via break-induced replication, meiotic DNA double-strand break formation	52
YOR182C	*rps30B*	protein biosynthesis	28
YPL106C	*sse1*	protein folding	48
YPL129W	*taf14*	G1-specific transcription in mitotic cell cycle, chromatin remodeling, transcription initiation from RNA polymerase II promoter	58
YPR072W	*not5*	poly(A) tail shortening, regulation of transcription from RNA polymerase II promoter	20
YPR135W	*ctf4*	DNA repair, DNA-dependent DNA replication, mitotic sister chromatid cohesion	92
YPR163C	*tif3*	translational initiation	62

*: Among those 8 parameters, the number of parameters where each mutant scored more abnormal value than drug-treated cells.

**:The number of parameters that identify significant differences with wild-type cells ($P < 0.0001$).

Table 6 Characterization of actin mutants in specific parameters

Parameter	CCV12-2_A1B	CCV109_A1B	DCV152_A1B	D14-3_C	DCV14-1_C	DCV108_C	D203	D206	the number of ○
Strain＼Num	235	112	519	2327	45	2429	18	380	
act1-112	○	○	○	○	×	×	○	○	6
act1-113	×	×	○	○	×	×	○	×	3
act1-117	○	×	○	○	×	×	×	×	3
act1-157	○	×	○	○	×	×	×	○	4

*Num: the number of the mutants which scored higher than the cells cultured in 1.5 μM LAT-A

○ indicates that that mutant scored more abnormal value than the cells treated with 1.5 μM LAT-A

× indicates that that mutant did'nt score more abnormal value than the cells treated with 1.5 μM LAT-A